Available online at www.sciencedirect.com
SCIENCE DIRECT®
International Journal of Thermal Sciences 44 (2005) 587–597
International Journal of Thermal Sciences
www.elsevier.com/locate/ijts

Spray forming: A numerical investigation of the influence of the gas to melt ratio on the billet surface temperature

N.H. Pryds [a], J.H. Hattel [b,*]

[a] *Materials Research Department, Risø National Laboratory, DK-4000 Roskilde, Denmark*
[b] *Process Modelling Group, Department of Manufacturing Engineering and Management, Technical University of Denmark, Building 425, DK-2800 Lyngby, Denmark*

Received 4 August 2004; accepted 17 January 2005

Abstract

The relationship between the gas to melt ratio (GMR) and the surface temperature of an evolving billet surface in spray forming is investigated numerically. The basis for the analysis is an integrated approach for modelling the entire spray forming process. This model includes the droplet atomisation taking thermal coupling into consideration and the deposition of material at the surface of the billet taking geometrical aspects such as shading into account. The coupling between these two models is accomplished by ensuring that the total droplet size distribution of the spray is the summation of "local" droplet size distributions along the r-axis of the spray cone. The criterion for a successful process has been a predefined process window characterised by a desired fraction solid range at a certain distance from the atomizer. Inside this process window, the gas and melt flows have been varied and the influence of the gas and metal flow rates on the surface temperature of the billet has been analysed. Based on this, a relationship for the surface temperature as function of the GMR has been suggested for the spray forming of a 100Cr6 billet.

Keywords: Spray forming; Atomization; Integrated modelling; Process optimization

1. Introduction

Despite a continuous attempt towards fundamental understanding of the spray forming process, many important features remain unexplored. An enhanced understanding of the process should permit development of predictive models elucidating the interrelationships between the process/structure/properties and performance.

The spray forming process has been continuously modelled and described in literature. The models are often divided into two parts namely: atomization and deposition. A major part of the models for atomization are based on the idea that the continuous phase affects the properties of the dispersed phase but not vice versa [1,2]. However, in a real system the droplets, which are represented by their size distribution do interact with each other via the gas and therefore a model that is able to reflect that, is desirable.

As for the deposition, the models proposed in literature can be divided into two principally different approaches, i.e. purely geometrical models [3–7] and models, which take both the thermal and the geometrical effect into consideration [8,9].

Recently, a new integrated model for both atomization and deposition in the spray forming process taking into account the interaction between the atomization gas and the different droplet sizes has been developed for a Gaussian shape [10–12] and billet shape [13] geometries.

When spray forming in industry, the surface temperature is an important process controlling parameter. The surface temperature is very much dependent on the energy contained in the droplets arriving to the surface of the preform, i.e. the temperature and size of the droplets. Moreover, the droplet size distribution as well as the temperature of the droplets

* Corresponding author. Tel.: +45 4525 4710, fax: +45 4593 4570.
E-mail address: jh@ipl.dtu.dk (J.H. Hattel).

1290-0729/$ – see front matter
doi:10.1016/j.ijthermalsci.2005.01.001

Nomenclature

a	experimentally determined temperature	K
a_{sp}	spray distribution parameter	$kg{\cdot}s^{-1}{\cdot}m^{-2}$
A	area	m^2
A_g	area of gas delivery nozzles	m^2
b	experimentally determined exponent	
b_{sp}	spray distribution parameter	m^{-2}
c_p^{gas}	specific heat capacity of gas	$J{\cdot}kg^{-1}{\cdot}K^{-1}$
c_p^{liq}	specific heat capacity of steel, liquid	$J{\cdot}kg^{-1}{\cdot}K^{-1}$
c_p^{sol}	specific heat capacity of steel, solid	$J{\cdot}kg^{-1}{\cdot}K^{-1}$
c_p^*	adjusted specific heat capacity of steel	$J{\cdot}kg^{-1}{\cdot}K^{-1}$
d	diameter of droplets	μm
d_m	mass mean diameter of droplets	μm
d_0	liquid stream diameter	μm
$d_{50,k}$	mass mean diameter of droplets in local distribution	μm
D_0	distance from the atomizer to the surface of the billet along the spray axis	m
f_l	fraction liquid	
f_s	fraction solid	
F_l	fraction liquid on preform surface	
$\dot{G}$	mass flow of gas	$kg{\cdot}s^{-1}$
GMR	Gas to Melt Ratio	
GMR_{high}	higher limit of the GMR range	
GMR_{low}	lower limit of the GMR range	
k	thermal conductivity	$W{\cdot}m^{-1}{\cdot}K^{-1}$
K_a	experimental constant in Eq. (1)	
l_e	eccentric distance from intersection point between line from atomizer at time = 0 and substrate	m
$\dot{m}$	mass flow of droplets	$kg{\cdot}s^{-1}$
$\dot{M}$	mass flow of melt	$kg{\cdot}s^{-1}$
n	experimental constant in Eq. (4)	
P_k^{local}	local droplet size distribution along r-axis	$W{\cdot}m^{-3}$
$\dot{Q}_{gen}$	source term in heat conduction equation	$W{\cdot}m^{-3}$
r	radius	m
SE	sticking efficiency	
t	time	K
T	temperature	K
T_E	eutectic temperature	K
T_{liq}	liquidus temperature	K
T_M	solvent melt temperature	K
T_{sol}	solidus temperature	K
$T_{surface}$	surface temperature of billet	K
v	withdrawal velocity of billet	$m{\cdot}s^{-1}$
v_0	initial gas velocity	$m{\cdot}s^{-1}$
v_g	gas velocity	$m{\cdot}s^{-1}$
We	Weber number	
x_0	reference value of the GMR	
x	space co-ordinate on surface of preform	m
y	space co-ordinate on surface of preform	m
z	space co-ordinate on surface of preform	m
z	distance from atomizer along the spray line	m

Greek symbols

α	experimental constant	
ε	parameter for SE	
η_g	kinematic viscosity of gas	Pa·s
η_l	kinematic viscosity of liquid	Pa·s
Δ	increment	
Δh	displacement of surface point during an increment	m
ΔH_f^{Left}	remaining latent heat after droplet flight	$J{\cdot}kg^{-1}$
ϕ	spray angle	°
λ_v	decay constant for gas velocity	m
ρ_g	density of gas	$kg{\cdot}m^{-3}$
ρ_s	density of steel	$kg{\cdot}m^{-3}$
σ_k	standard deviation	μm
θ	angle in cylindrical co-ordinate system in preform	°
ξ	shading function	

Others

i	droplet group	
k	control volume index in r-direction	
$\mathbf{e}$	unit vector	m

are dependent on the ratio between the gas flow and the melt flow and on the gas velocity. A way to control the surface temperature during the process, is to control the ratio between the flow rates of the gas and the melt known as the gas to melt ratio (GMR).

In the present work, the recent developed integrated numerical model for the spray forming process [12,13] has been used to study the influence of the GMR on the surface temperature. On the basis of the calculations, a relationship between the GMR and the surface temperature is suggested for the 100Cr6 sprayed billet.

2. Model description

The model used in this work includes the droplet atomisation taking thermal coupling into account and the deposition of material at the surface of the billet taking geometrical considerations such as shading into account. The coupling between these two models is accomplished by ensuring that the total droplet size distribution of the spray is the summation of "local" droplet size distributions along the r-axis. The atomisation model is based on a 1-dimensional, quasi-steady formulation of the spray cone [10] whereas

the thermal analysis of the preform in the deposition model is based on a finite volume solution of the 3-dimensional heat conduction equation in cylindrical coordinates [12,13]. The atomisation model involves only thermal coupling, i.e. the droplets interact with each other via the gas, whereas they do not interact "momentum-wise", i.e. the droplet velocity is affected by the gas only and hence not by other droplets. The details of the different sub-models and validations against analytical and numerical solutions as well as experimental observations have been extensively published and can be found elsewhere, e.g. [9–13]. However, some of the basic assumptions of the models are shortly presented.

2.1. Atomization model

During atomization, a bulk liquid is disintegrated into droplets of different sizes. Looking at a given atomizer design and melt composition, several variables influence the droplet size distribution which in turn is decisive for the thermal state of the arriving droplets at the preform and hence the surface temperature. These variables include process related variables such as: Melt superheat, nozzle geometry, melt flow rate, gas flow rate, gas velocity, gas temperature, and chemical and physical properties of the liquid metal and the atomization gas [1].

In order to solve correctly the two-phase flow problem, i.e. the gas phase and the liquid metal phase, during the atomisation process, a fully coupled momentum and energy formulation should be applied in general. In the present model, the momentum and energy conservation of the droplets during flight are coupled together. The droplet size distribution is discretized by a number of size groups ranging from 1 up to 600 μm in diameter with a constant increment of Δd. The upper limit is chosen as the maximal possible size of the droplets in the distribution. Each group's contribution to the overall heat balance is given by its mass flow, i.e. its probability times the total mass flow of metal, $\dot{M}$, see Eq. (3).

The heat balance between the droplets and the surrounding gas is set up by assuming a 1-D Eulerian frame, i.e. fixed finite control volumes along the centreline of the spray cone, assuming that the injected gas is only slightly expanded along the radial direction. This assumption enables to simulate the process in one dimension, see Fig. 1. It should be noted that thermal coupling was present in the atomization model, because of the fact that the gas temperature was not assumed to be known a priori, but calculated together with the droplet temperatures in a coupled manner. A more comprehensive description of the atomization model is given in [10–13].

The mean diameter of the droplet size distribution is directly affected by the GMR and several suggestions for this relationship have been given in literature. In the present model, the following empirical equation representing the mass median diameter has been used [14]:

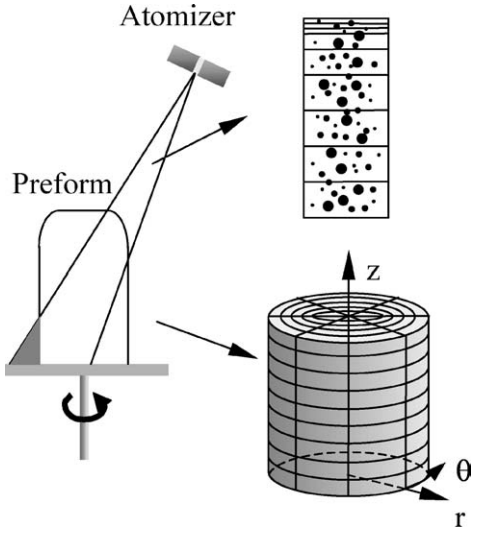

Fig. 1. Integrated model of the spray forming process consisting of a 1-D model of the atomization in the spray cone and a 3-D model of the deposition process.

$$\frac{d_m}{d_0} = K_a\left[\frac{\eta_l}{\eta_g We}\left(1+\frac{\dot{M}}{\dot{G}}\right)\right]^{0.5} \tag{1}$$

where d_m is the mass median diameter of the droplets, d_0 is the liquid stream diameter, K_a is a constant depending on the experimental conditions and $\dot{M}$ and $\dot{G}$ are mass flow rates of the liquid and gas, respectively, and *We* is the Weber number. From this expression it is readily seen that increasing the GMR decreases the mass median diameter and thereby the droplet size. The temperature of the arriving particles at the deposit surface depend both on the particle size, i.e. smaller droplets cool faster than large ones, as well as on the position of the deposit substrate along the axis of symmetry. This leads to an enthalpy of the spray cone, which is position dependent and influences the surface temperature of the billet.

In order to achieve a good homogeneous and dense billet, the desirable fraction solid of the particles on impact should be around 0.5–0.7 [1]. This criterion defines the desired process window used later on in the analysis.

2.2. Deposition model

The deposition model is based on a 3-D cylindrical geometry, (r,θ,z), see Fig. 1. The temperatures in the spray deposit material are thus governed by

$$\rho_s c_p^{\mathrm{sol}}\frac{\partial T}{\partial t} = \frac{\partial}{\partial r}\left\{k\frac{\partial T}{\partial r}\right\} + \frac{1}{r}k\frac{\partial T}{\partial r} + \frac{1}{r^2}\frac{\partial}{\partial \theta}\left\{k\frac{\partial T}{\partial \theta}\right\} + \frac{\partial}{\partial z}\left\{k\frac{\partial T}{\partial z}\right\} + \dot{Q}_{\mathrm{gen}} \tag{2}$$

In the present case $\dot{Q}_{\mathrm{gen}}$ arises from the phase change. Note that the release of the remaining latent heat after droplet

flight, ΔH_f^{Left}, in the preform, is accomplished by introducing an adjusted value for the specific heat, c_p^*, according to the expression $c_p^* = c_p^{\text{sol}} - \Delta H_f^{\text{Left}} \frac{\partial f_s}{\partial T}$, where the term $\frac{\partial f_s}{\partial T}$ is given by the Clyne–Kurz model. The derivation of c_p^* is easily obtained by setting $\dot{Q}_{\text{gen}}$ equal to the released heat per unit volume from solidification in Eq. (2). Combining this temperature dependent c_p^*-value with an algorithm "pushing" the temperature back to the liquidus temperature when entering the solidification interval, no iterations are needed for this non-linearity in order to ensure consistency between temperatures and material data.

The numerical solution of Eq. (2) is based on the finite volume method, in which the governing differential equation is integrated over each of the control volumes. This way, the conservation principle, i.e. energy balance is expressed for the control volume. Further details on the choice of boundary conditions and heat transfer coefficients are given elsewhere [13].

2.3. Coupling of the models

The coupling of the atomization and the deposition model is achieved through the droplet size distribution. The total size distribution of the spray is in fact the summation of a number of "local" distributions along the r-axis. The mesh along the r-axis is divided into control volumes each of which contains a droplet size distribution, $P_k^{\text{local}}(d_i)$, i.e. a "local" distribution. The overall mass distribution can be expressed as

$$\begin{aligned}
&\dot{m}\left(d \in \left[d_i - \frac{\Delta d}{2}; d_i + \frac{\Delta d}{2}\right]\right) \\
&\quad = \dot{M} \sum_k \int_{\ln(d_i - \frac{\Delta d}{2})}^{\ln(d_i + \frac{\Delta d}{2})} P_k^{\text{local}}(d_i) d(\ln d_i) \\
&\quad \approx \dot{M} \sum_k P_k^{\text{local}}(d_i) \Delta(\ln d_i) \\
&\quad = \dot{M} \sum_k \frac{1}{\sigma_k \sqrt{2\pi}} \exp\left(\frac{-(\log d_i - \log d_{50,k})^2}{2\sigma_{kj}^2}\right) \\
&\qquad \times \left(\log\left(d_i + \frac{1}{2}\Delta d\right) - \log\left(d_i - \frac{1}{2}\Delta d\right)\right)
\end{aligned} \tag{3}$$

where the local dispersion is assumed to depend on the local mass mean similarly to the global distribution, i.e. $\sigma_k = \sqrt[3]{\frac{d_{50,k}}{13}}$ [12].

The local size distribution, i.e. in each control volume, is then used to calculate the average enthalpy of each control volume. The major advantage of the atomization model is that it enables a calculation of the enthalpy for each group of similar droplet size, based on the interaction of this size group with the whole range of sizes and the surrounding gas. The enthalpy of the different droplet sizes is then contributing to the overall enthalpy of the specific control volume. Subsequently, the enthalpy is converted into temperature and used to describe the temperature of the specific cell. For more details on this procedure see [13].

A key parameter, which determines the yield and the shape of the deposited material, is the sticking efficiency, *SE* of the droplets to the surface. The sticking efficiency describes how good the droplets "stick" to the already deposited material. The model proposed by Mathur [8] was applied for the numerical procedure. This *SE* model is based on two macroscopic components: (a) a geometrical component which depends on the angle of incident between the spray direction and the surface normal and (b) a thermal component which depends upon the fraction liquid in the spray and the fraction liquid in the deposited surface. The thermal $SE(T)$ is given by

$$SE(T) = (f_s \alpha_s + f_l \alpha_L)\varepsilon \tag{4}$$

where

$$\alpha_s = 1 - 0.75 \cdot (1 - F_L) \quad \text{and} \quad \alpha_l \approx 0.98 \tag{5}$$

and the parameter ε varies from 0 to 1 and is consistent with the variation in the viscosity as a function of F_L.

2.4. Billet shape model

The spray forming process in the industry is used mainly for the production of billet shape products. The final billet shape and its properties are strongly influenced by the process parameters and therefore the ability to control the final shape is very important.

The billet model in the present work describes the evolution of a 3D deposit surface in Cartesian coordinates. The important effect of shading has to be incorporated into the model in order to simulate the correct shape of the billet, see Fig. 1.

The billet shape model is initiated by assigning a number of grid points to the substrate surface and thereby defining a mesh, composed of triangles. The position of these grid points is then advanced with time. In each time step of the calculation, the new position of all the points on the surface is calculated using the mass flow distribution and geometrical considerations. The new position is found as [7], see Fig. 2

$$\begin{aligned}
x_{\text{new}} &= x + \Delta h \cdot \mathbf{e}_n \cdot \mathbf{e}_x \\
y_{\text{new}} &= y + \Delta h \cdot \mathbf{e}_n \cdot \mathbf{e}_y \\
z_{\text{new}} &= z + \Delta h \cdot \mathbf{e}_n \cdot \mathbf{e}_z
\end{aligned} \tag{6}$$

where

$$\Delta h = \int_t^{t+\mathrm{d}t} \xi(x, y, x, t) \cdot \dot{M}(r, z) \cdot \mathbf{e}_n \cdot \mathbf{e}_f \, \mathrm{d}t \tag{7}$$

$\dot{M}(r, z)$ is the mass flux and $\xi(x, y, z, t)$ is the shading function which is designed in such a way that ξ is equal to 0 when shading is present, otherwise it is 1.

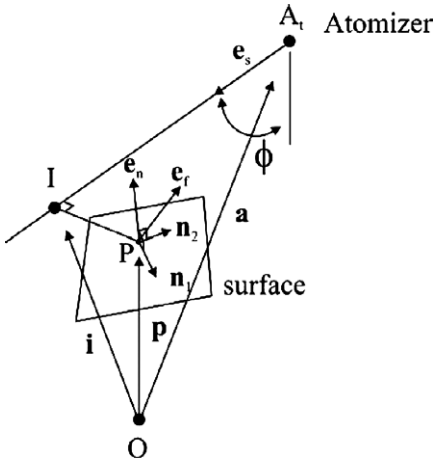

Fig. 2. Vectors describing the evolution of the billet surface.

In order to calculate the surface evolution, i.e. Δh, the four terms, $\mathbf{e}_f$, $\mathbf{e}_n$, $\dot{M}$ and ξ must be obtained. The vectors $\mathbf{e}_f$ and $\mathbf{e}_n$ are obtained from relatively straightforward vector calculus, see [13]. The mass flow at any point at the surface of the preform can be found from the mass distribution in the spray cone in combination with the actual positions of the atomizer and the point under consideration [13].

The mass distribution used in the present model is an axis symmetrical Gaussian expression

$$\frac{\dot{M}}{A} = a_{\mathrm{sp}} \exp\left(-b_{\mathrm{sp}} r^2\right) \tag{8}$$

where r is the shortest distance from a point to the symmetry axis line (spray axis) and a_{sp} [kg·s^{-1}·m^{-2}] and b_{sp} [m^{-2}] are spray distribution parameters which depend on the total mass flow, the design of the atomizer and the distance from the nearest point on the spray axis to the atomizer (the spray distance).

Integration of Eq. (8) yields the total mass flow in the spray cone

$$\dot{M} = \int_0^{\infty}\int_0^{2\pi} a_{\mathrm{sp}} \exp\left(-b_{\mathrm{sp}} r^2\right) r \,\mathrm{d}\theta \,\mathrm{d}r = \frac{\pi a_{\mathrm{sp}}}{b_{\mathrm{sp}}} \tag{9}$$

This expression is used later on when establishing the different calculation cases.

The determination of the shading function, ξ, calls for a rather complex algorithm. This has recently been published [13].

3. Calculation cases

One of the important control parameters for achieving a good billet is the fraction solid of the spray. In order to achieve a good homogeneous and dense billet, the desirable fraction solid on impact should be around 0.5–0.7 [1]. The material chosen for the present analysis was a steel 100Cr16, see Table 1 and the atomization gas was Nitrogen, Table 2.

Table 1
Material properties for the 100Cr16 steel

Solidus temperature T_{sol} [K]	1570
Liquidus temperature T_{liq} [K]	1724
Solvent melt temperature T_M [K]	1811
Eutectic temperature T_E [K]	1419
Density ρ_s [kg·m^{-3}]	7810
Specific heat of solid c_p^{sol} [J·kg^{-1}·K^{-1}]	640
Specific heat of solid c_p^{liq} [J·kg^{-1}·K^{-1}]	724

Table 2
Material properties of the N_2 gas

Density ρ_g [kg·m^{-3}]	1.5
Viscosity η_g [Ns·m^{-2}]	0.000032
Specific heat c_p^{gas} [J·kg^{-1}·K^{-1}]	1000
Thermal conductivity k [W·m^{-1}·K^{-1}]	0.026

The geometrical process parameters are given in Table 3. In order to investigate the influence of the GMR on the surface temperature of the billet, different parameters were varied during the study. A basic atomizer geometry was chosen according to a melt stream diameter of $d_0 = 3700$ μm and an area of gas delivery nozzles of $A_g = 0.0003$ m^2. Using this geometry the melt flow was varied between the values of 0.05, 0.1 and 0.2 kg·s^{-1}, see Table 3, for the three studied cases 1, 2.1 and 3.1, respectively. Assuming a mass distribution parameter b_{sp} of 1000 m^{-2}, the other parameter, a_{sp} can be found from Eq. (9) as 15.915 kg·s^{-1}·m^{-2}, 31.83 kg·s^{-1}·m^{-2} and 63.66 kg·s^{-1}·m^{-2} for the three cases of 1, 2.1 and 3.1, respectively, see Table 3. The GMR was then varied between a fixed lower limit of 1.0 and a varying upper limit, i.e. GMR of 2.0, 2.5 and 3.0 for the three cases, respectively. This results in a range of gas flows of 0.05–0.1, 0.1–0.25 and 0.2–0.6 kg·s^{-1}, for the three cases, see Table 3. Note that since the area of the gas delivery nozzles (A_g) is kept constant for cases 2.1 and 3.1 as compared to case 1, the gas velocity increases proportionally to the increasing gas flow for these cases according to Eq. (10).

$$v_g = \frac{\dot{G}}{\rho_g A_g} \exp(-z/\lambda_v) \tag{10}$$

where v_g is the gas velocity and the decay constant varies approximately with the initial gas velocity as [15]

$$\lambda_v = \alpha v_0^n \tag{11}$$

and the two constants, α and n, have been experimentally determined as 3×10^{-4} and 1.24–1.25, respectively [15].

This procedure of keeping the nozzle geometry constant while increasing the melt flow means that the gas velocity in especially case 3.1 becomes very high at the exit of the nozzle, ranging from 444 to 1333 m·s^{-1}. In the upper end of this interval the velocities become unrealistically high. Bearing this in mind, the next step of the calculations was carried out with changed nozzle geometry. Thus, two new calculation cases were established in which the melt stream

Table 3
The process parameters used for the calculations

Calculation case	1	2.1	2.2	3.1	3.2
Melt flow $\dot{M}$ [kg·s^{-1}]	0.05	0.1	0.1	0.2	0.2
Gas to Melt Ratio GMR	1.0–2.0	1.0–2.5	1.0–2.5	1.0–3.0	1.0–3.0
Gas flow $\dot{G}$ [kg·s^{-1}][a]	0.05–0.1	0.1–0.25	0.1–0.25	0.2–0.6	0.2–0.6
Mass distribution parameter a_{sp} [kg·s^{-1}·m^{-2}]	15.915	31.83	31.83	63.66	63.66
Mass distribution parameter b [m^{-2}]	1000	1000	1000	1000	1000
Change in atomizer geometry	No	No	Yes	No	Yes
Liquid stream diameter d_0 [μm]	3700	3700	5232	3700	7400
Area of gas delivery nozzles A_g [m^2]	0.0003	0.0003	0.0006	0.0003	0.0012
Rotation velocity ω [rot·min][b]	116	116	116	116	116
Spray angle ϕ [deg]	35	35	35	35	35
Eccentric distance from intersection point between line from atomizer at time = 0 and substrate, l_e [m]	0.02	0.02	0.02	0.02	0.02
Distance from atomizer to rotation axis along the spray axis, D_0 [m]	0.5	0.5	0.5	0.5	0.5
Withdrawal velocity v	c	c	c	c	c
Constant in Eq. (1), K_a	50	50	50	50	50

[a] As shown, the GMR was varied between 1–2, 1–2.5 and 1–3 in the three cases, respectively. For the prescribed melt flows this results in the shown gas flows.
[b] The rotation velocity is chosen to be 116 rot·min^{-1} since literature suggests that this should be high enough to ensure rotational symmetry [6].
[c] The withdrawal velocity is chosen in such a way that the distance D_0 is maintained at 0.5 m at all times. This is done in order to keep the solid fraction of the droplets arriving to the surface of the deposit as constant as possible.

diameter and the area of gas delivery nozzles were varied. These cases that are based on cases 2.1 and 3.1 are named 2.2 and 3.2 and are referred to as the modified geometry. The variation was made in such a way to ensure that the gas velocity at the exit of the atomizer was the same as in case 1 and the GMR variation range remained unchanged as compared to cases 2.1 and 3.1. Hence, the names 2.2 and 3.2.

From Eq. (10), it is readily seen that enforcing a constant gas velocity results in the gas area being proportional to the gas flow. Thus, using a metal flow rate of 0.05 kg·s^{-1} and a nozzle area of 0.0003 m^2 as reference, i.e. case 1 (and keeping in mind that the GMR range should remain unchanged as compared to cases 2.1 and 3.1), melt flow rates of 0.1 and 0.2 kg·s^{-1} result in a nozzle area of 0.0006 and 0.0012 m^2 in cases 2.2 and 3.2, respectively. Since the gas velocity is assumed to be the same as in case 1, the increase in melt flow is accounted for by increasing the melt flow diameter. This was then adjusted to 5232 and 7400 μm for the metal flow rates of 0.1 and 0.2 kg·s^{-1} in cases 2.2 and 3.2, respectively, see Table 3.

4. Numerical results

Fig. 3(a)–(c) show the calculated solid fraction as a function of distance from the atomizer. In these figures, the four vertical and horizontal lines correspond to the distance from the atomiser and the solid fraction of the spray, respectively. These lines represent the limit values of the process parameters. The fraction solid is marked with two lines, 0.45 is set as the lower limit and 0.75 is set as the upper limit. The distance from the atomizer in which the substrate is situated is also marked with two lines—one at a distance of 0.5 m and one at a distance of 0.6 m—typical distances used in the industry [16].

As seen from Fig. 3(a)–(c), increasing the melt mass flow rate causes an increase in the fraction solid for the non-modified case. On the other hand for the modified case increasing the melt mass flow rate causes a decrease in the fraction solid. However, this decrease is not as pronounced as was the increase in the non-modified case. Moreover, it is seen that, if the atomizer geometry is kept constant, i.e. without modifying the nozzle dimensions, the fraction solid of the spray for a mass flow of 0.1 kg·s^{-1} is above the desirable fraction solid for a $GMR = 1.5$ (Fig. 3(b)) and a $GMR = 2.0$ (Fig. 3(c)). In the case of a mass flow of 0.2 kg·s^{-1} in the non-modified case, the fraction solid already exceeds the limits at a $GMR = 1.0$ (Fig. 3(a)) and for a $GMR = 1.5$ (Fig. 3(b)) it is far above the limit and approaching a fraction solid of 1.

Modifying the nozzle geometry improves the process with respect to staying inside the process window. Only in Fig. 3(a) for a GMR of 1.0, the modified case of a mass flow of 0.2 kg·s^{-1} is below the desirable fraction. This indicates that modifying the nozzle geometry the proposed way makes the process less sensitive to changes in the GMR as compared to the original nozzle geometry.

Fig. 4 shows the fraction solid at a distance of 0.5 m as a function of the different GMRs. The fraction solid increases with increasing GMR. For the non-modified cases, increasing the mass flow rate causes an increase in the fraction solid. Already after a GMR of 1.5, the desirable fraction solid for the spray is exceeded for mass flow rates of 0.1 and 0.2 kg·s^{-1}. However, for the modified cases the solid fraction decreases slightly with increasing mass flow, as men-

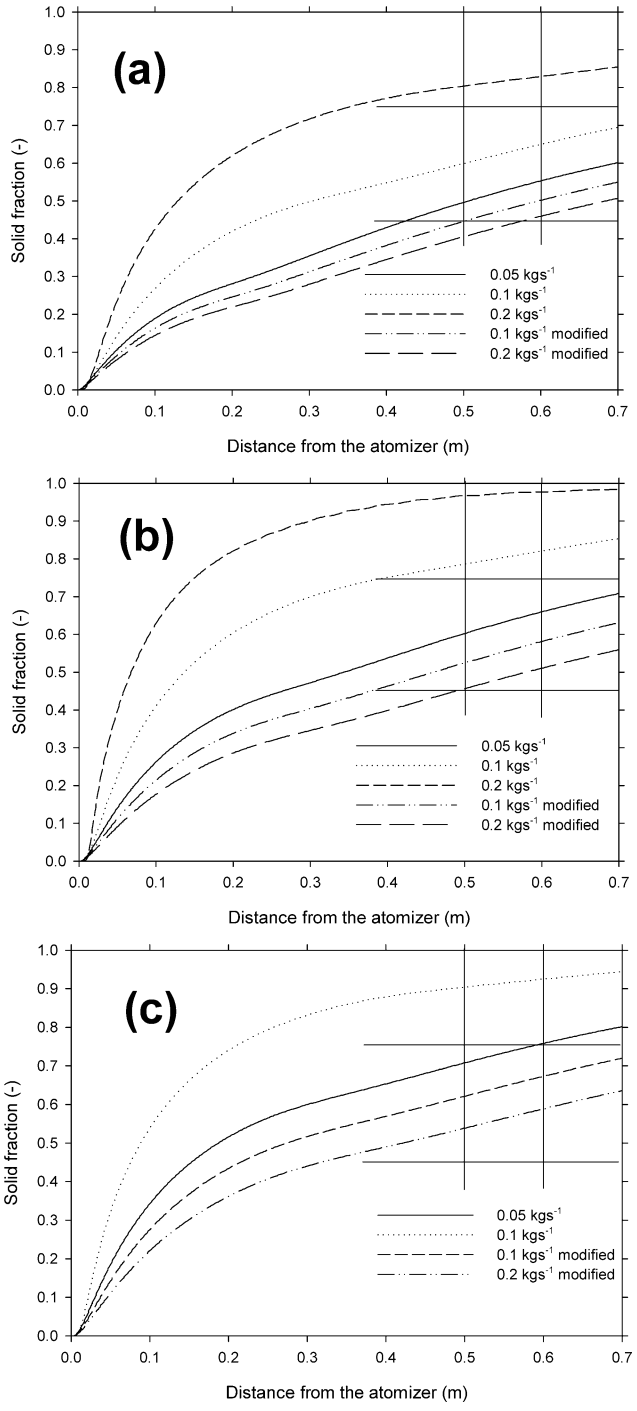

Fig. 3. Average fraction solid of the spray as function of distance from atomizer and mass flow for: (a) $GMR = 1$, (b) $GMR = 1.5$ and (c) $GMR = 2$.

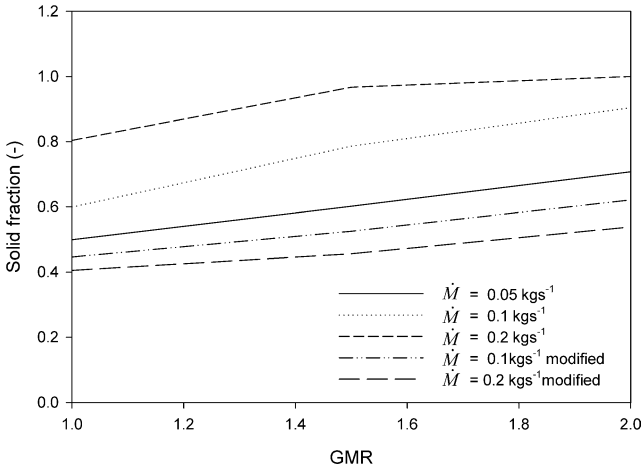

Fig. 4. Average fraction solid at a distance of 0.5 m from the atomizer as a function of GMR for the different mass flows.

Table 4
Constants in Eq. (12) obtained as best curve-fit

Calculation case	1	2.2	3.2
a [K]	1597.32	1627.30	1644.57
b	7.09	6.37	4.51
x_0	3.04	3.97	6.02

Table 5
Constants in Eq. (12) obtained from Eqs. (13)–(15)

Calculation case	1	2.2	3.2
GMR_{low}	1	1	1.5
GMR_{high}	2	2.5	3
a from Eq. (13) [K]	1588	1619	1636
b from Eq. (14)	7.48	6.23	4.9
x_0 from Eq. (15)	3	4	6

tioned before, but it remains within the predefined process window when the GMR is in the range of 1.5–2.

Fig. 5(a)–(c) show the fraction solid as a function of the distance from the atomizer for different values of the GMR and constant mass flow rates of 0.05, 0.1 and 0.2 kg·s^{-1}, respectively. Fig. 5(a) represents case 1, i.e. non-modified data with a flow rate of 0.05 kg·s^{-1}. Fig. 5(b) and (c) represent the modified nozzle data, i.e. cases 2.2 and 3.2 in Table 3. The calculations were made in order to evaluate which values of the GMR fit the process window, hence the incremental stepping of 0.25 in the figures. As seen in Fig. 5(a) for a mass flow of 0.05 kg·s^{-1} and a GMR varying from 1 to 2, the fraction solid of the spray is within the desirable range, whereas for a mass flow of 0.1 kg·s^{-1}, the fraction solid is in the desirable range for $GMR = 1$–2.5 (Fig. 5(b)). For a mass flow of 0.2 kg·s^{-1} the range of GMR is varying from 1.5 to 3 within the desirable process window (Fig. 5(c)). These GMR ranges define the terms GMR_{low} and GMR_{high}, see Table 5. These terms are explained further in the discussion.

It is seen from Fig. 5(a)–(c), that the range of acceptable GMRs, in which the solid fraction has the desirable value, i.e. 0.45–0.75, is larger with an increasing mass flow.

5. Definition of the billet surface temperature

In order to determine the effect of the GMR on the surface temperature, it was decided to investigate the top surface billet temperature only. This is due to the fact that the numerical calculations, not surprisingly, show that the billet surface temperature is affected at the top surface only by the arriv-

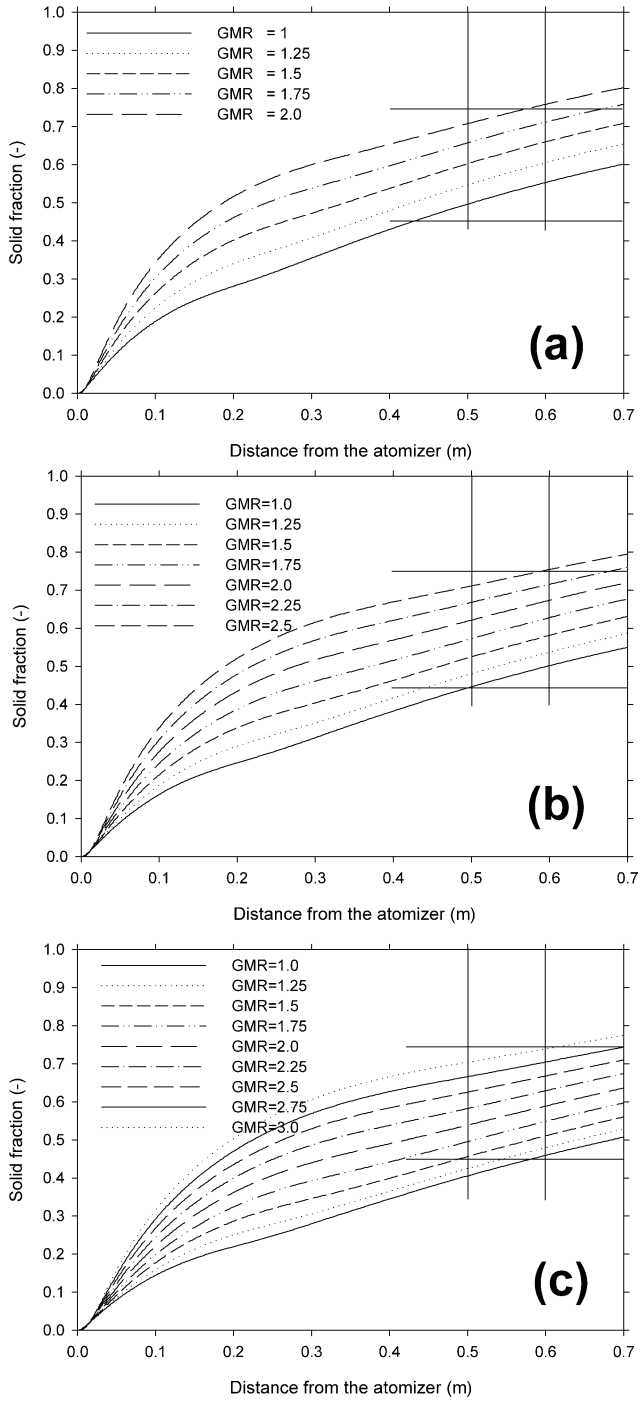

Fig. 5. Average fraction solid of the spray as function of distance from atomizer and GMR. (a) Mass flow of 0.05 kg·s^{-1}. Non-modified nozzle data, calculation case 1; (b) Mass flow of 0.1 kg·s^{-1}. Modified nozzle data, calculation case 2.2; (c) Mass flow of 0.2 kg·s^{-1}. Modified nozzle data, calculation case 3.2.

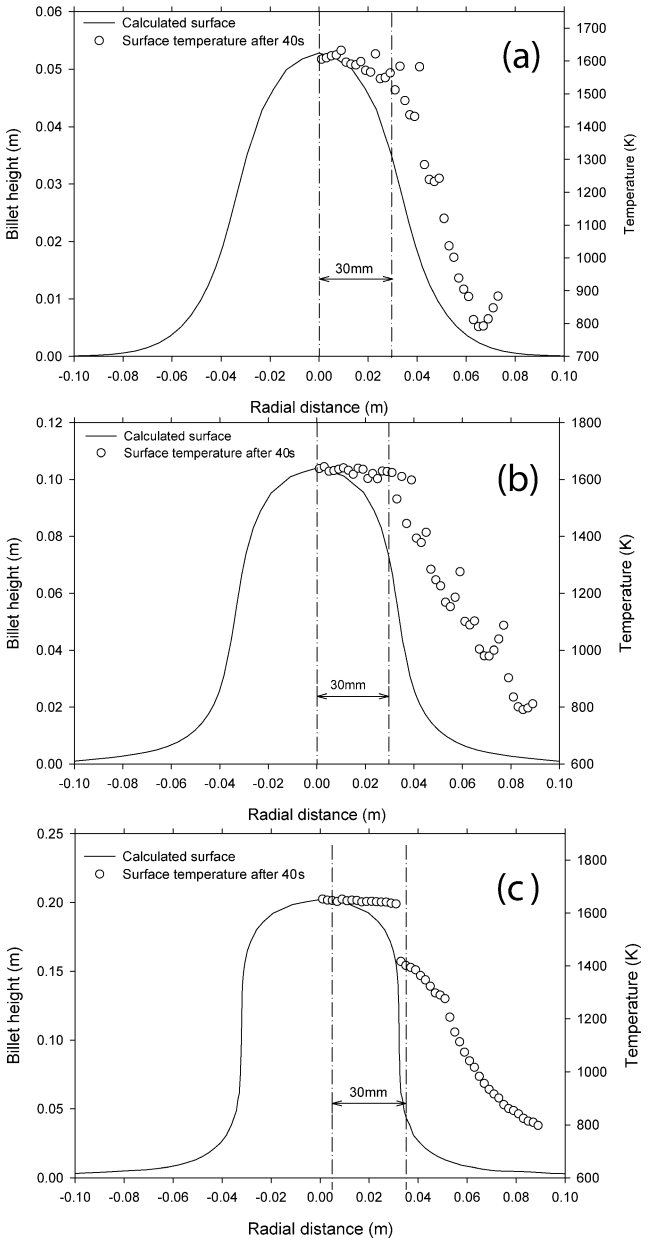

Fig. 6. Shape of the surface and the temperature of the surface after 40 s. (a) $GMR = 1.5$ and mass flow of 0.05 kg·s^{-1}, non-modified nozzle data, calculation case 1; (b) $GMR = 1.5$ and mass flow of 0.1 kg·s^{-1}, modified nozzle data, calculation case 2.2; (c) $GMR = 1.5$ and mass flow of 0.2 kg·s^{-1}, modified nozzle data, calculation case 3.2.

ing particles, whereas the surface temperature on the side of the billet is almost unaffected by a varying GMR. This means that even though, the side temperature of the billet is of course accounted for in the model because it is a full 3-dimensional analysis, it has no relevance for the success of the deposition that takes place at the top of the billet and hence it is not taken into account when defining the term "surface temperature" for the purpose of the present work.

Since the temperatures of the top surface affect the growth rate of the billet, the thermal field within the billet, and as a consequence of those, the microstructure and the properties of the billet, these phenomena will be closely related to the choice of GMR.

The shapes of the billets after 40 s are shown in Fig. 6(a)–(c) for a constant GMR of 1.5 and varying the melt mass flow only. The deposition time was chosen to be 40 s since above this time, a quasi-stationary state is reached in all the calcu-

lation cases. A GMR of 1.5 was chosen as this value yielded results within the desired process window for all the three values of melt flow, i.e. 0.05, 0.1 and 0.2 kg·s^{-1}. Fig. 6(a)–(c) are presented in order to show why, when calculating the average surface temperature; only the surface within the radial distance of 0.03 m is used. Looking at the temperature distribution in all three figures, it is realized that the temperature is approximately constant up to a radial distance of 0.03 m from the billet centre line. The surface temperature has a value of approximately 1600 K at the top surface and it decreases along the radial distance, i.e. above a distance of 0.03 m, to a value of about 800 K at a distance of 0.09 m from the centre. Since the top surface temperature of the billet, i.e. up to a distance of 0.03 m from the centre, is found to be relatively constant, the surface temperature was defined as the average value of the temperatures at the top surface within a radius of 0.03 m.

It can also be observed from Fig. 6(a)–(c) that the shape of the billets continuously changes from a Gaussian to a cylindrical like shape. The reason for this change is a result of differences in the mass flow rate, e.g. the mass flow in Fig. 6(c) is 4 times as large as in Fig. 6(a).

As seen in Fig. 6(a), the temperature profile indicates that the change of the temperature with distance is not smooth. These jumps in temperature are due to the discrete nature of the numerical method where a control volume is filled at a certain time step. The jumps in the temperatures represent control volumes, which have recently been filled. In Fig. 6(c) no such jumps are seen. The explanation for this is that the outer areas of the billet in this case are so far away from the atomizer, that practically no melt is deposited; hence no control volumes are filled.

6. Discussion

The droplet size distribution depends on the GMR, so that increasing the GMR, the mean diameter of the overall droplet distribution decreases. This is seen from Eq. (1). It was therefore expected that the surface temperature decreases with increasing GMRs since the fraction solid of the spray increases with increasing GMR, see Fig. 5(a)–(c). Figs. 7–9 show the surface temperatures as a function of the GMR at different mass flow rates and times. The surface temperature decreases with increasing GMR, although the rate of changes is very small in the lower end of the GMR range.

The correlation between the GMR and the surface temperature in all three cases is assumed to follow an equation of the following form

$$T_{\text{surface}} = \frac{a}{(1 + (GMR/x_0)^b)} \tag{12}$$

where a, b and x_0 are constants depending on the process parameters. a is a temperature [K] and x_0 corresponds to a reference value of the GMR. b is a dimensionless exponent.

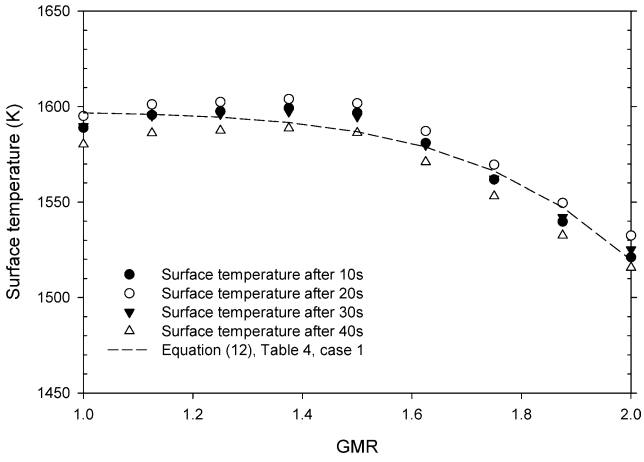

Fig. 7. Surface temperature as function of GMR. The equation for the best fit to the surface temperature, Eq. (12) using the constants in Table 4, is marked with the curved line. Mass flow of 0.05 kg·s^{-1}. Non-modified nozzle data, calculation case 1.

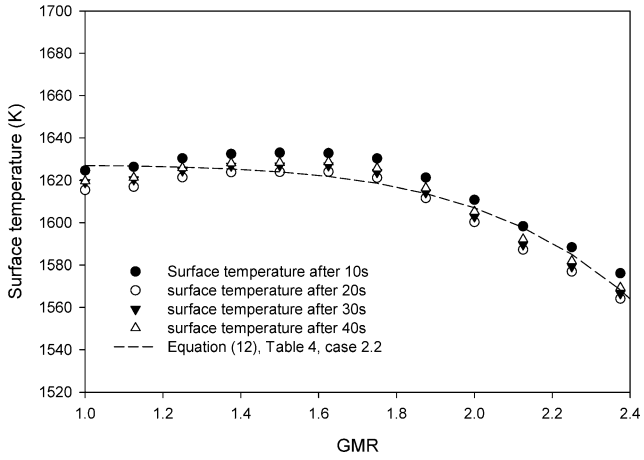

Fig. 8. Surface temperature as function of GMR. The equation for the best fit to the surface temperature, Eq. (12) using the constants in Table 4, is marked with the curved line. Mass flow of 0.1 kg·s^{-1}. Modified nozzle data, calculation case 2.2.

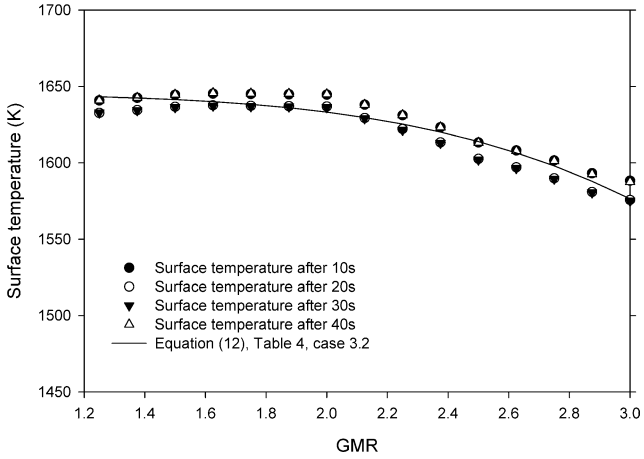

Fig. 9. Surface temperature as function of GMR. The equation for the best fit to the surface temperature, Eq. (12) using the constants in Table 4, is marked with the curved line. Mass flow of 0.2 kg·s^{-1}. Modified nozzle data, calculation case 3.2.

In each of the three calculation cases, i.e. case 1, 2.2 and 3.2, the parameters, a, b and x_0 which result in the best fit of Eq. (12) with the calculated data points are given in Table 4.

The three investigated cases are too few to draw real solid and general conclusions from regarding the behaviour of the surface temperature with the GMR in general, i.e. for a wide range of alloys and spraying conditions. However, the present work can be considered as a first attempt to establish a correlation from which at least the tendencies can be drawn for the particular case under consideration, i.e. spray forming a billet of 100Cr6 within a narrow process window.

The numerical simulations performed with the model indicate that for the present case, the simple relationship between the GMR and the surface temperature as given by Eq. (12) should involve knowledge about the interval of GMR for which the atomizer provides a fraction solid within the desirable range of 0.45–0.75. The limits of this GMR-interval are denoted GMR_{low} and GMR_{high}. For the calculation cases considered in the present work, the values of these limits are found from Fig. 5(a)–(c) for the cases 1, 2.2 and 3.2, respectively. This results in the GMR-intervals of 1.0–2.0, 1.0–2.5 and 1.5–3.0. These values are also given in Table 5. Moreover, the simulations indicated that the numerically predicted surface temperature as defined in the previous section for a GMR equal to both the lower limit and the higher limit of the GMR in the range should be contained in the relationship as well. These are denoted $T(GMR_{\text{low}})$ and $T(GMR_{\text{high}})$.

For the constant a in Eq. (12), the following is found

$$a = T(GMR_{\text{low}}) \tag{13}$$

where $T(GMR_{\text{low}})$ is the surface temperature for the GMR equal to the lower limit of the range, as mentioned before. In Table 5, the constant a based on Eq. (13) is shown. The surface temperature is found by taking an average over the 4 temperatures representing the different times. Comparing the a-values in Table 5 with the ones in Table 4 shows that Eq. (13) approximates the best curve-fit of Eq. (12) quite well for the constant a.

For the exponent, b, the following relationship is found:

$$b = \frac{T(GMR_{\text{low}}) - T(GMR_{\text{high}})}{10 \cdot (GMR_{\text{high}} - GMR_{\text{low}})} + (GMR_{\text{high}} - GMR_{\text{low}}) \tag{14}$$

Here $T(GMR_{\text{high}})$ is the surface temperature for a GMR equal to the higher limit of the range, GMR_{high}.

The exponent is a measure of how the surface temperature decreases with increasing GMR, so it makes sense to assume that the exponent is dependent on the range of GMR and the temperature difference between $T(GMR_{\text{low}})$ and $T(GMR_{\text{high}})$. Different attempts of combining these were made and Eq. (14) was found to give the best results, see Tables 5 and 4 for comparison with the best-fit values regarding the exponent b.

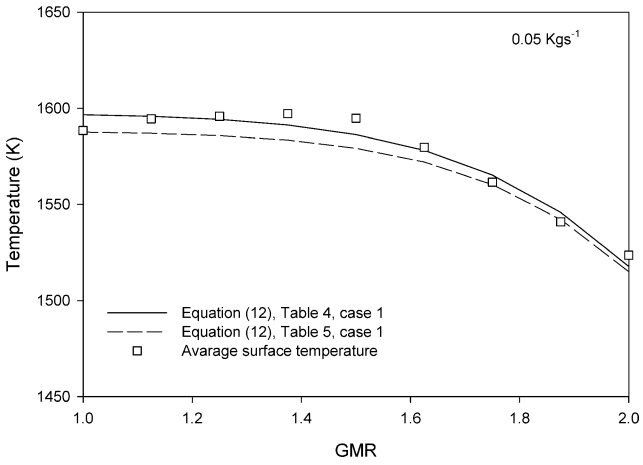

Fig. 10. Surface temperature as function of GMR. Both Eq. (12) using Table 4, Eq. (12) using Table 5 and the average surface temperature are shown. Mass flow of 0.05 kg·s^{-1}. Non-modified nozzle data, calculation case 1.

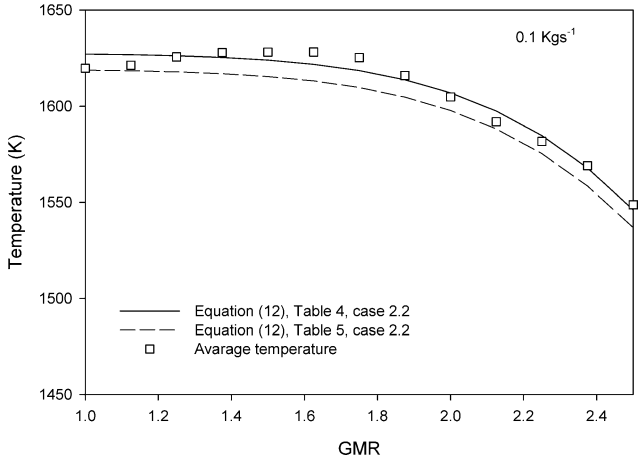

Fig. 11. Surface temperature as function of GMR. Both Eq. (12) using Table 4, Eq. (12) using Table 5 and the average surface temperature are shown. Mass flow of 0.1 kg·s^{-1}. Modified nozzle data, calculation case 2.2.

In Eq. (12) x_0 can be interpreted as a constant describing a reference GMR. x_0 is assumed to depend on the GMR and the following is found from the numerical calculations:

$$x_0 = GMR_{\text{high}}^2 - (GMR_{\text{high}} + GMR_{\text{low}}) \tag{15}$$

The results for x_0 obtained from Eq. (15) are listed in Table 5.

In Figs. 10–12, the best fits for Eq. (12) using the constants in Table 4 are shown together with results from Eqs. (13)–(15) as shown in Table 5. The average surface temperature is shown as well. The average temperature plotted in these figures is found from taking the average temperature at four different deposition times 10, 20, 30 and 40 s.

In Figs. 10 and 11, it is seen that the shapes of the curves with the modified equation are similar to the original; the differences seem to be the level of the curves, which is related to a. In Fig. 12 the level also seems to be too low in the lower range of the GMR, whereas the curvature is different

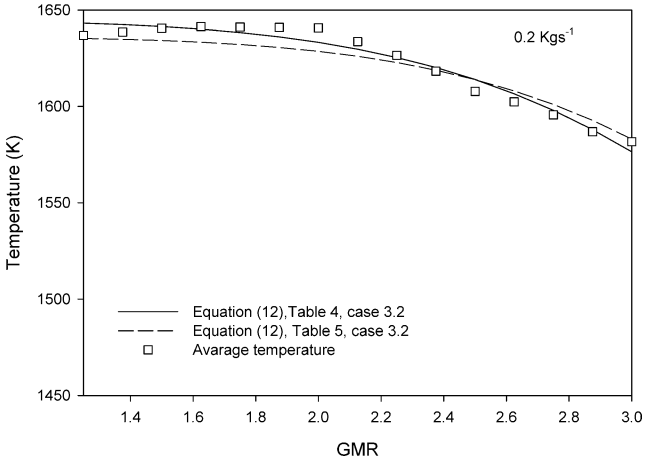

Fig. 12. Surface temperature as function of GMR. Both Eq. (12) using Table 4, Eq. (12) using Table 5 and the average surface temperature are shown. Mass flow of 0.2 kg·s^{-1}. Modified nozzle data, calculation case 3.2.

and the two curves intersect each other. This is related to the value of b.

The found correlations are strictly valid only for the cases under consideration; however, one could expect that the structure of the equations will be similar for other materials. The actual values of the constants in the equations would on the other hand be expected to be different. The proposed approach for the derivation of the correlations, however, is still valuable, because it is more generic in the sense that it could certainly be used for other cases of spray forming also.

7. Conclusion

In the present work, the relationship between the gas to melt ratio (GMR) and the surface temperature of an evolving billet surface in the spray forming process has been investigated numerically. This has been done with an integrated approach, which models the entire process taking both atomisation and deposition into account. A correlation between the GMR and the surface temperature has been proposed in which three constants depending on process conditions have been introduced. The correlation is found from only three cases, which generally speaking are too few to draw general conclusions from, however, at least the tendencies for the case under consideration, i.e. spray forming billets of 100Cr6 within a narrow process window, can be drawn from the proposed correlation. In this sense, the present work constitutes a first example of using a comprehensive integrated numerical model involving both atomization and deposition for the purpose of quantitatively analysing the very important relationship between GMR and surface temperature in spray forming.

References

[1] Y. Zhou, Y. Wu, E.J. Lavernia, Process modeling in spray deposition: A review, Internat. J. Non-Equilibrium Processing 10 (1997) 95–183.
[2] C.T. Crowe, M. Sommerfeld, Y. Tsuji, Multiphase Flows with Droplets and Particles, CRC Press, Boca Raton, FL, 1997.
[3] I.A. Frigaard, Dynamics of spray-formed billets, SIAM J. Appl. Math. 55 (5) (1995) 1161–1203.
[4] I.A. Frigaard, Spraying the perfect billet, SIAM J. Appl. Math. 57 (3) (1997) 649–682.
[5] I.A. Frigaard, Growth dynamics of spray-formed aluminium billets Part I: Steady state crown shapes, J. Mat. Proc. Manufacturing Sci. 3 (1994) 173–193.
[6] H.-K. Seok, H.C. Lee, K.H. Oh, J.-C. Lee, H.-I. Lee, H.Y. Ra, Formulation of rod-forming models and their application in spray forming, Metall. Mat. Trans. A 31 (2000) 1479–1488.
[7] H.-K. Seok, D.-H. Yeo, K.H. Oh, H.-I. Lee, H.Y. Ra, A three-dimensional model of the spray forming method, Metall. Mat. Trans. B 29 (1998) 699–708.
[8] P.C. Mathur, S. Annavarapu, D. Appelian, A. Lawley, An integral model for process understanding and control, Mat. Sci. Engrg. A 142 (1991) 261–276.
[9] D. Bergmann, U. Fritsching, Sequential thermal modelling of the spray-forming process, Internat. J. Thermal Sci. 43 (4) (2004) 403–415.
[10] J.H. Hattel, N.H. Pryds, J. Thorborg, P. Ottosen, A quasi-stationary numerical model of atomized metal droplets. Part I: Model formulation, Modelling Simul. Mater. Sci. Engrg. 7 (3) (1999) 413–430.
[11] N.H. Pryds, J.H. Hattel, J. Thorborg, A quasi-stationary numerical model of atomized metal droplets. Part II: Prediction and assessment, Modelling Simul. Mater. Sci. Engrg. 7 (3) (1999) 431–446.
[12] N.H. Pryds, J.H. Hattel, T.B. Pedersen, J. Thorborg, An integrated numerical model of the spray forming process, Acta Mater. 50 (16) (2002) 4075–4091.
[13] J.H. Hattel, N.H. Pryds, A unified spray forming model for the prediction of billet shape geometry, Acta Mater. 52 (18) (2004) 5275–5288.
[14] H. Lubanska, Correlation of spray ring data for gas atomization of liquid metals, J. Metals 22 (1) (1970) 45–49.
[15] P.S. Grant, B. Cantor, L. Katgerman, Modeling of droplet dynamic and thermal histories during spray forming I: Individual droplet behaviour, Acta Metall. Mater. 41 (11) (1993) 3097.
[16] P. Kjeldsteen, personal communication, Danspray, 2002.